Journal of Applied Mechanics Vol.10, pp.77-88 (August 2007) JSCE

Damage detection in concrete structures using tunable piezoelectric actuators

Shuichi Mikami*, Sherif Beskhyroun**, Tomoyuki Yamazaki***, Toshiyuki Oshima****
三上修一*, シェリフ ベスキロウン**, 山崎智之***, 大島俊之****

*Associate Professor, Dept. of Civil Eng., Kitami Institute of Technology, (165 Koen-cho, Kitami, 090-8507)
**Postdoctoral Fellow, Dept. of Civil Eng., Kitami Institute of Technology, (165 Koen-cho, Kitami, 090-8507)
***Assistant Professor, Dept. of Civil Eng., Kitami Institute of Technology, (165 Koen-cho, Kitami, 090-8507)
****Professor, Dept. of Civil Eng., Kitami Institute of Technology, (165 Koen-cho, Kitami, 090-8507)

In this study, the state of the art of modal parameters-shift-based damage identification is advanced by incorporating a tunable piezoelectric actuator into the structure to enrich the modal parameters measurements, meanwhile implementing an identification algorithm to sufficiently utilize the enriched information. By integrating tunable piezoelectric actuators into the structure, we can introduce additional resonant peaks into the system dynamic response in the frequency domain, and these additional peaks can be adjusted over the frequency band by tuning the actuator. Clearly, a significantly increased amount of modal parameters shift information can be expected to reflect the damage effect. A series of analyses using a reinforced concrete (RC) wall and a RC column integrated with a tunable piezoelectric actuator is carried out to demonstrate this proposed methodology and verify the performance. The results indicate that piezoelectric actuator has high potential applicability to damage assessment of concrete structures.

Key Words: damage detection, piezoelectric actuators, vibration data, health monitoring

1. Introduction

Structural health monitoring and damage identification has received much attention in recent years due to its significance and broad applications in civil, mechanical and aerospace engineering communities. Based on the information provided by the detection system, immediate changes to the current operating procedure and environment can be proposed to maintain structural integrity, and plans on future maintenance can also be scheduled to elongate the service life of the structure. Many techniques, such as ultrasonic and acoustic emission methods, magnet field methods and eddy-current methods, have been developed for damage detection; however, these local detection methods require that the vicinity of the damage be known and the portion of the structure being damaged is accessible for inspection. On the other hand, the vibration-based damage identification approaches utilize the global structural responses, and thus often do not require the direct accessibility to the damaged spot, which could be advantageous in many applications. The basic idea of vibration-based damage identification is that damage in the structure will change the structural properties (mass, stiffness or damping) and these changes will result in changes in the dynamic characteristics of the global structural responses, such as natural frequencies, damping ratio and mode shapes. A significant amount of work has been performed for detecting structural damages using basic modal properties: resonant frequency[1-4], measured mode shapes[5-7], mode shape curvature[8-10], and dynamically measured flexibility[11-13]. One may refer to Doebling et al[14,15] and Cornwell et al[16] for comprehensive reviews on vibration-based damage identification methods.

Among all the vibration-based damage identification methods, the information carriers most frequently used are the modal frequency change (eigenvalue change) and the mode shape change (eigenvector change). When using the sensitivity-based model updating approaches for damage identification, usually both the modal frequency and mode shape measurements are needed to reconstruct the stiffness and mass parameters of the structure. However, only few modes can be measured experimentally. Moreover, it is difficult to achieve high accuracy in mode shape measurement[17]. In comparison, the resonant frequencies are much easier to measure and less sensitive to measurement noises[18]. Nevertheless, in current practices, the frequency-shift-based damage identification methods have severe limitations. One major issue is that the number of natural frequencies

that can be measured is normally much smaller than the number of degrees of freedom required for accurate damage identification. In order to increase the modal frequency data available for sensitivity-based model updating, several methods have been proposed in the literature. Cha and Gu[19] explored a mass addition technique to enrich the modal information measurement. They showed that the mass matrix can be corrected by adding known masses to the structure and measuring its new modal data, and then the stiffness matrix can also be updated by requiring the associated eigenvalue problem to have the same modal information as that measured for the new mass-added system. Nalitolela et al[20] also studied the feasibility of using added mass/stiffness to extract additional resonant frequencies. It is worth mentioning that the direct addition of mass/stiffness to a structure might be difficult for many applications and may encounter physical restrictions. Later, Lew and Juang[21] introduced the concept of a virtual passive controller to enrich the modal frequency measurement. Output feedback controllers are incorporated into the structure to generate additional closed-loop modal frequencies. In this approach, while no physical mass or stiffness is attached to the structure, it requires a certain amount of external input energy as a controller source and the incorporation of a feedback controller could introduce additional disturbance into the system.

This paper aims at advancing the state of the art of the modal parameters-shift-based damage identification method by using the electro-mechanical system integration characteristics of piezoelectric actuators. The basic idea of this new approach is to implement a tunable piezoelectric actuator to the structure to be monitored. The piezoelectric actuator with tunable wave function generator can introduce additional resonant frequencies at arbitrary frequency bands, and one can obtain a family of spectral response functions by tuning the wave function generator to different values. By this feature, one will obtain a much enriched modal measurement that can capture the damage-induced variation of the system dynamic response more completely and accurately. Analyses are carried out on a RC column and RC wall to demonstrate the effectiveness and performance improvement. It is shown that the modal response can be enriched by actuator tuning, which leads to a much more accurate identification of damage.

2. New idea of integrating tunable piezoelectric actuators

Piezoelectric materials have been explored extensively for structural dynamics applications because of their electromechanical coupling characteristics. The direct effect of producing an electrical charge when stressed mechanically has been often used in sensors to sense the structural deformation, while the converse effect of producing a mechanical strain under electrical field has been used in actuators to alter the dynamics response of the structural system. Due to such two-way electro-mechanical coupling, piezoelectric materials have been widely used for both active and passive vibration control applications. In a purely active arrangement, electrical field or charge is applied to the piezoelectric actuators (either surface bonded to or embedded in the host structure) to generate control force/moment. In a passive situation, an external shunt circuit is usually integrated to the piezoelectric material[22-24]. Shunting the piezoelectric materials, on the other hand, does not preclude the simultaneous use of the shunted piezoelectric materials as active actuators[25]. In fact, a well designed active–passive hybrid piezoelectric actuator network[26-29] not only could enhance the active control authority, but also could increase the system's passive damping.

In this research, a piezoelectric actuator is used to excite the test structures with several excitation frequencies but the excitation wave and the excitation amplitude are not changed. The wave function generator shown in Fig. 1 is used to adjust the required excitation frequency range, the time in which the actuator reaches the maximum frequency and the excitation wave form. Then, the adjusted wave is transferred to the power supplier (Fig. 2) which in turn provides the actuator (Fig. 3) with the adjusted power. The actuator is fixed to the structure by a magnetic holder. The magnetic holder is suitable in case of fixing the actuator to steel structures; however, a thin steel plate must be mounted on the surface of concrete structures to attach the magnetic holder. A steel spring is fixed over the actuator to control the excitation force amplitude. Main characteristics of the equipments used in this research are shown in Table (1). Fig. 4 shows an example of the produced force by the actuator. As can be shown in figure, the excitation frequency is gradually increasing over time until it reaches its maximum value after the designated time (15 seconds in this example). In this example, the excitation wave form is a sweep function. It should also be noted that because the actuator is pressed but not glowed to the test structure, the actuator provides pressure force only.

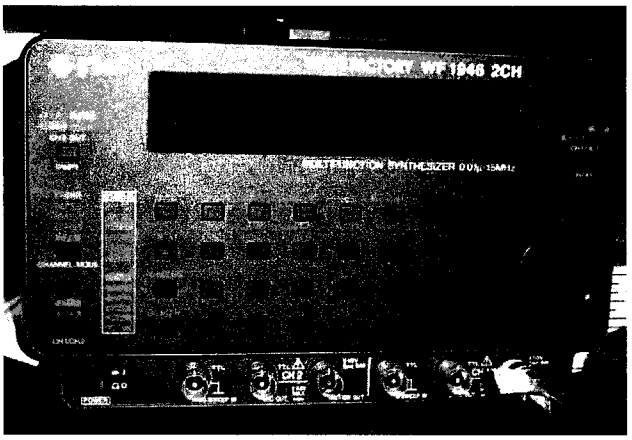

Fig. 1 Wave function generator

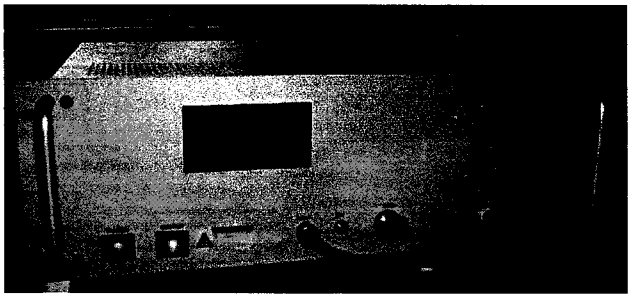

Fig. 2 Power supplier

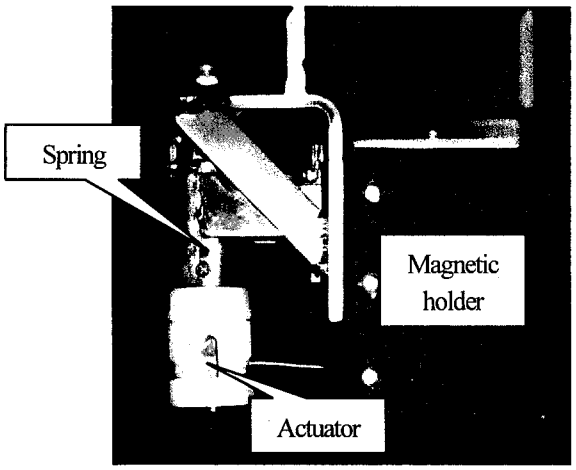

Fig. 3 Piezoelectric actuator

Table 1 Equipment characteristics

Piezoelectric actuator	
Dimensions (W×T×H)	10×10×20 (mm)
Min. and Max. Freq.	0~982 Hz
Displacement (100V)	12.3 μm
Max Force	350 N
Wave function generator	
Min. and Max. Freq.	0.01μHz~15MHz
Max. Output Volt	20Vp-p/OPEN, ±10V/OPEN
Power source	
Max. Power	150V

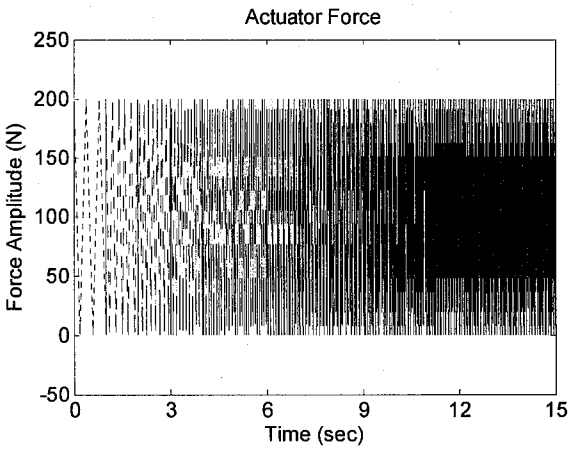

Fig. 4 Simulation of the actuator force

3. Damage detection: theoretical aspects

3.1 Definition of spectral functions

For a continuous time series, $x(t)$, defined on the interval of 0 to T, the Discrete Fourier Transform (DFT), $X(f)$, is defined as[31]

$$X(f) = \int_0^T x(t) e^{-i2\pi ft}\, dt \tag{1}$$

where $i = \sqrt{-1}$, and

f= cyclic frequency (Hz).

This function is complex and its magnitude is typically plotted in engineering units (EU), such as m/s^2 or g, versus frequency. The power spectrum is then defined as

$$|X(f)|^2 = X(f)X^*(f) \tag{2}$$

where * denotes a complex conjugate. The power spectrum is a real-valued frequency domain function with units of (EU)^2. The power spectral density (PSD), $G_x(f)$ is defined as

$$G_x(f) = \frac{2}{T} E\left[|X(f)|^2\right] \tag{3}$$

where $E[\ ]$ indicates an ensemble average for a specific f over n samples of $X(f)$.

The cross spectral density (CSD), $G_{xy}(f)$, relating two time histories, $x(t)$ and $y(t)$ is defined as

$$G_{xy}(f) = \frac{2}{T} E\left[X^*(f)Y(f)\right]. \tag{4}$$

CSD is a complex function. The CSD is calculated from node point accelerations at any reading channel $x(t)$ relative to a reference reading $y(t)$ using MATLAB[32-34] standard and MATLAB Signal Processing Toolbox.

3.2 Modal Assurance Criterion (MAC)

Next to the basic modal parameters of structures such as eigenfrequencies, modal damping ratios and mode shapes, some derived coefficients obtained from these parameters can also be useful for damage detection in structures. The MAC[35] factor may be mentioned in this category. This factor is derived from mode shapes and expresses the correlation between two measured mode shapes obtained from two sets of tests. The MAC factor being linked to mode shapes, sufficient number of degrees of freedom (number of measurement points) are needed to obtain accurate quantities. The next paragraph gives a short theoretical description of the MAC factor.

MAC compares two modes using the orthogonality properties of the mode shapes. The MAC that compares mode i and j has the form

$$MAC(i,j) = \frac{\left|\sum_{k=1}^{n} (\phi_j)_k (\phi_i)_k^*\right|^2}{\left[\sum_{k=1}^{n} (\phi_j)_k (\phi_j)_k^*\right]\left[\sum_{k=1}^{n} (\phi_i)_k (\phi_i)_k^*\right]} \tag{5}$$

where n is the number of measuring points, $(\phi)_k$ is an element of the mode-shape vector and the asterisks denote complex conjugate. In practice, MAC value greater than 0.9 indicates correlated modes and value less than 0.05 indicates uncorrelated modes.

As illustrated previously, only few modes can be measured experimentally which may decrease the accuracy of damage identification algorithms that use this parameters. In this research, MAC will be used to compare CSD data measured at each frequency component rather than comparing mode shapes. In such technique, large sets of dynamic response data can be obtained with much less calculation effort. CSD data, measured at different measuring channels at the same frequency component f, construct one vector

which can be called operational mode shape. These data are called operational mode shapes because they are estimated at each frequency component in the measurement range rather than at the peak components. In this research, MAC value will be computed using CSD data instead of using mode shapes as follows:

- The acceleration time history is measured at each sensor location and one sensor is used as a reference.
- CSD is estimated from the time history response at each sensor relative to the time history response at the reference. CSD can be estimated in the frequency range of 0-F_s , where F_s = sampling rate / 2. The total measurement frequency range (0-F_s) is then divided to a number of frequency components.
- In Eq. (5), CSD data measured at different measuring points at each frequency component represent $(\phi_i)_k$ where ϕ represents CSD data instead of mode shape data, i represents the frequency component at which CSD data is measured, and k represents the channel number ($k = 1$: number of measuring channels).

MAC can be used to compare CSD data of two different sets of data obtained from the undamaged structure to examine the repeatability of the experiment, as will be explained in more details later. MAC can also be used to compare CSD data obtained from the undamaged and damaged structures to detect the occurrence of damage. Changes in MAC values that results from noise and measurement errors will be compared to those resulting from damage.

In case of comparing two sets of response data obtained from the same structure's state (e.g. undamaged state) after repeating the experiment, MAC can be utilized as follows:

- In Eq. (5), CSD data measured at different measuring points at any frequency, f, for the first test, $\{CSD_f\}_1$, simulate i^{th} mode (ϕ_i). CSD data measured at the same frequency f but for the second test, $\{CSD_f\}_2$, simulate j^{th} mode (ϕ_j).
- At any frequency component, f, in the measurement range from f_1 to f_m, a MAC value close to unity indicates that CSD data obtained from the two tests are similar or close. Consequently, it can be assumed that the influence of noise or measurement errors is small at this frequency component.
- On the other hand, a MAC value that is far from unity indicates a great disparity in the CSD data. Hence, CSD data, at this frequency component, is assumed to be sensitive to noise and measurement errors.

In the same manner, MAC can be used to compare CSD data obtained from the intact structure with CSD data obtained from the damaged one. MAC values close to unity will indicate that no damage is detected and MAC values close to zero will indicate the presence of damage. It is, therefore, very important to distinguish between the changes in MAC that result from damage from those changes that result from the presence of noise or measurement errors.

4. Experiment setup

The experimental work in this research was carried out on a RC column and a RC wall. The column main dimensions and layout are shown in Fig. 5. One piezoelectric actuator was used for exciting the structure and eight accelerometers were used to measure the acceleration response in the horizontal direction. The locations of the actuator and accelerometers are shown in Fig. 5. The issue of choosing the best sensor locations is not investigated in this study; however, the actuator and accelerometers should be distributed on the test structure in such a way that satisfies some important conditions. The actuator must be located close to the most suspected area of damage to excite various modes in this area. If the suspected area of damage is difficult to predict, the actuator should be placed in a location that gives the highest structure's response. The accelerometers should cover large area of the monitored structure but, at the same time, the vibration induced by the actuator force, which is relatively small, must reach the farthest accelerometer. Two damage cases were introduced to the lower part of the column in the opposite side of the sensors (photo in Fig. 5) and are summarized as follows:

- Case 1 (D1): Removing a concrete block of 50 cm height, 42 cm length and 12 cm depth, as shown in the photo in Fig. 5.
- Case 2 (D2): The same as case 1 + cutting the steel bars shown in Fig. 5.

Damage size in case 1 is big and can be easily detected using many damage identification methods. However, damage in case 2 is relatively small compared to case 1 and the change in the structure response between these two cases will be investigated in this paper. In other words, case 1 will be considered as the intact state and case 2 will be considered as the damaged state.

Several excitation frequency ranges were used to excite the test structure in the intact state as well as in each damage case. The basic idea of using different excitation frequency ranges is that for every structure and for every damage case (different damage type, size and location) there always exist some modes of vibration that are more sensitive to this specific damage case than other modes. These sensitive modes depend on the structure geometry, damage type, damage location, damage severity, influence of noise, and several other effects. It is very difficult to determine in prior the most sensitive modes for a specific structure with a specific damage case. Therefore, it was decided to excite the structure with different frequency bands assuming that one of these frequency bands will be the most effective in detecting a specific damage.

Small damage changes the structure's response in a localized area and introduces almost no change in the global behavior of the structure. These localized changes in the structure's response usually affect the higher modes of vibration. Many published papers have concluded that higher modes are usually more sensitive to damage than lower modes. Therefore, it was decided to excite the test structures with high frequency ranges from 300 to 800 Hz. The first excitation frequency range was 300-400 Hz. The experiment was repeated three times in each damage state. The same previous procedures were performed for the following excitation frequency range of: 400-500 Hz, 500-600 Hz, 600-700 Hz, and 700-800 Hz. The second tested structure in this research is the concrete wall. Basic dimensions, layout and sensors locations are shown in Fig. 6.

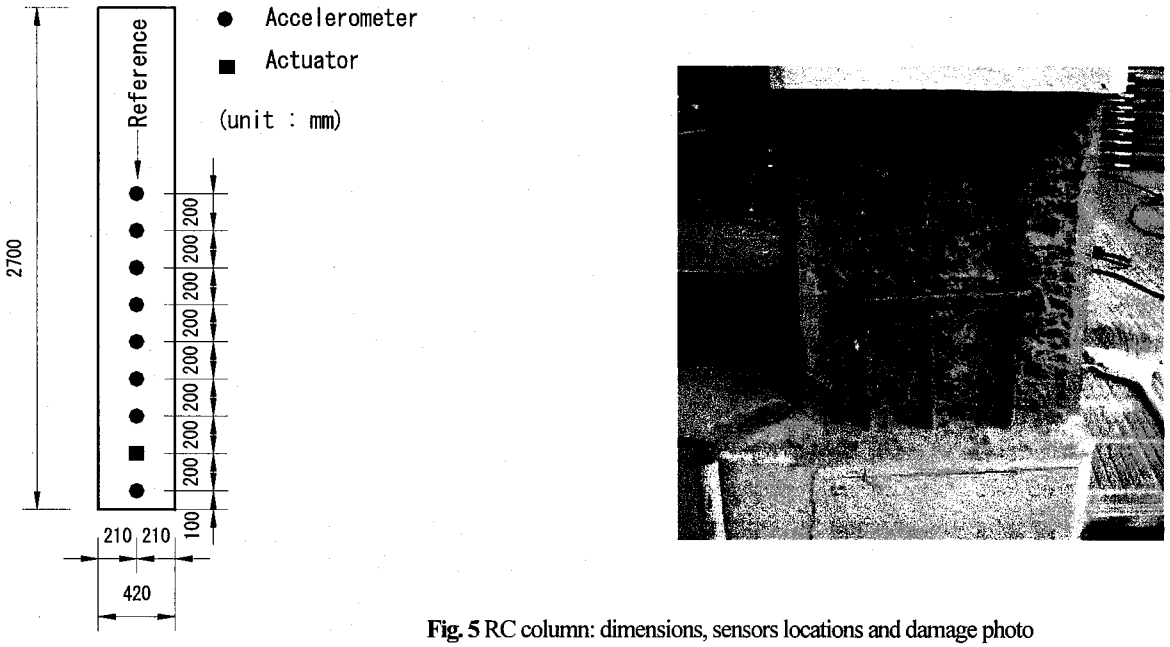

Fig. 5 RC column: dimensions, sensors locations and damage photo

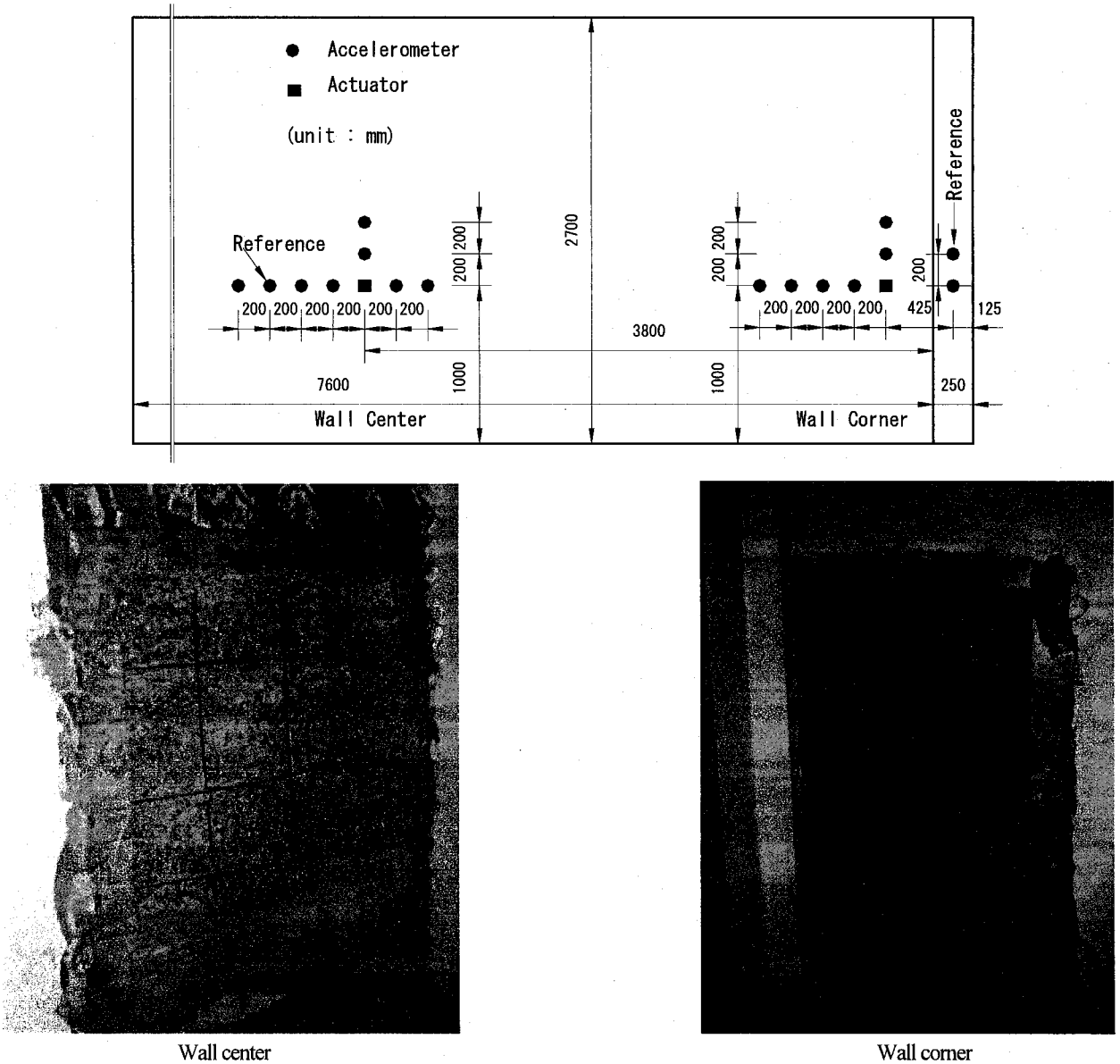

Wall center

Wall corner

Fig. 6 RC wall: dimensions, sensors locations and damage photos

The experiment was carried out in two different locations; the center and one corner of the wall. The following damage cases were introduced to center location:

- Case 1 (D1): Removing a concrete block of 100 cm height, 100 cm width and 10 cm depth.
- Case 2 (D2): The same as case 1 + cutting the steel bars shown in Fig. 6.

As illustrated in column structure, only the relative damage between case 1 and 2 will be investigated in this study.

The following damage cases were introduced to corner location:

- Case 1 (D1): Removing a concrete block of 100 cm height, 72 cm width and 11 cm depth.
- Case 2 (D2): The same as case 1 + cutting the steel bars.

The relative damage between case 1 and 2 will be investigated for the corner location. The experiment was performed as explained in column structure.

5. Damage identification results

5.1 The RC column structure

CSD data is calculated from the acceleration data at each measuring channel relative to a reference channel. Channel number 8 from the bottom of the column is chosen as a reference (Fig. 5). Any measuring channel can be used as a reference for other channels. The influence of changing the reference location is not investigated in this study. A typical acceleration response at channel 2 for damage case 1 and test 1 using excitation range of 500-600 Hz is shown in Fig. 7.

As explained previously, the experiment is repeated three times for each excitation range and each damage case. Fig. 8 shows the magnitude (square root of the square value of real part plus the square value of imaginary part) of CSD between channels 2 and 8 for three sets of acceleration data obtained from damage case 1 (test 1 [D1], test 2 [D1], and test 3 [D1]) using an excitation frequency range of 500-600 Hz. As clearly indicated in this figure, the structure's response in the frequency range of 500-600 Hz (excitation frequency range) is much higher than the response at any other frequency range. This feature is very effective in reducing the influence of noise and measurement errors, as will be explained later in this section. Another observation in this figure is that the structure's response changes at almost every frequency component due to repeating the experiment without introducing any damage to the current state (assuming that damage case 1 is the intact state). These changes are obviously due to the presence of noise and measurement errors in the measured experimental data. When CSD is estimated between other channels relative to the reference channel after changing the excitation frequency range, similar observations are made. The structure's peak response is always noticed within the excitation frequency band. From this observation it can be shown that the tunable piezoelectric actuator could introduce additional resonant frequencies at the excitation frequency bands. In Fig. 8, the frequency axis is divided using a step of 5 Hz and at each frequency component, MAC is computed for each two sets of CSD data measured at various measuring points. For example, CSD data at the frequency component 530 Hz estimated at different channels $\{CSD_{530}(1,8), CSD_{530}(2,8), \ldots, CSD_{530}(8,8)\}$ construct one operational mode shape ϕ_i (i = 530). CSD data obtained at the same frequency component (f = 530 Hz) but for another test (or another damage case) represent ϕ_j. Real and imaginary values of CSD data estimated at the frequency component 530 Hz for three different sets of data obtained from damage case 1 using excitation frequency range of 500-600 Hz are shown in Fig 9 (a), (b), respectively. The following step is to compare every two sets of data {test 1 – test 2} & {test 1 – test 3} & {test 2 – test 3} using MAC. A single MAC value is obtained by comparing each two sets of data. Each resulting MAC value represents one point at the frequency component 530 Hz and each combination is represented by different line type, as shown in Fig. 10. The same procedures are applied at each frequency component in the total measurement range (0-2000 Hz) to draw Fig. 10.

Figs. 10 and 11 show MAC values for three combinations of CSD data; {test 1 [D1] - test 2 [D1]}, {test 1 [D1] - test 3 [D1]}, and {test 2 [D1] - test 3 [D1]} using excitation frequency range of 500-600 Hz and 600-700 Hz, respectively. In Fig. 10, it is clear for all three combinations that MAC value is close to unity in the frequency range of 500 to 600 Hz (i.e. excitation range), which indicate very stable data and very small influence of noise and measurement errors in this range. On the other hand, small values of MAC in other frequency ranges indicate big difference in CSD between different tests.

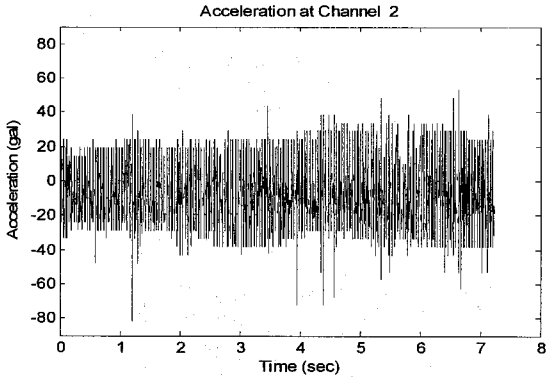

Fig. 7 A typical acceleration response at channel 2 for damage case 1 and test 1 using excitation frequency range of 500-600 Hz

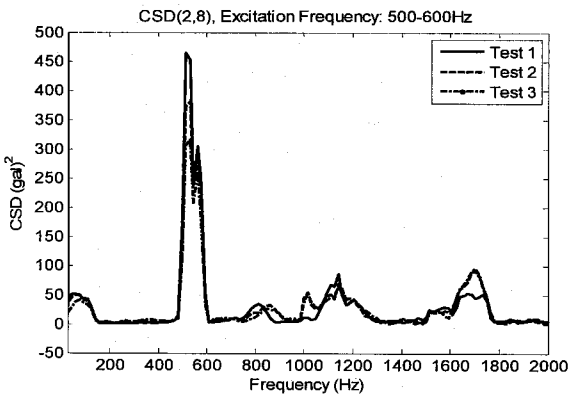

Fig. 8 CSD for three sets of acceleration data obtained from damage case 1 using excitation frequency range of 500-600 Hz

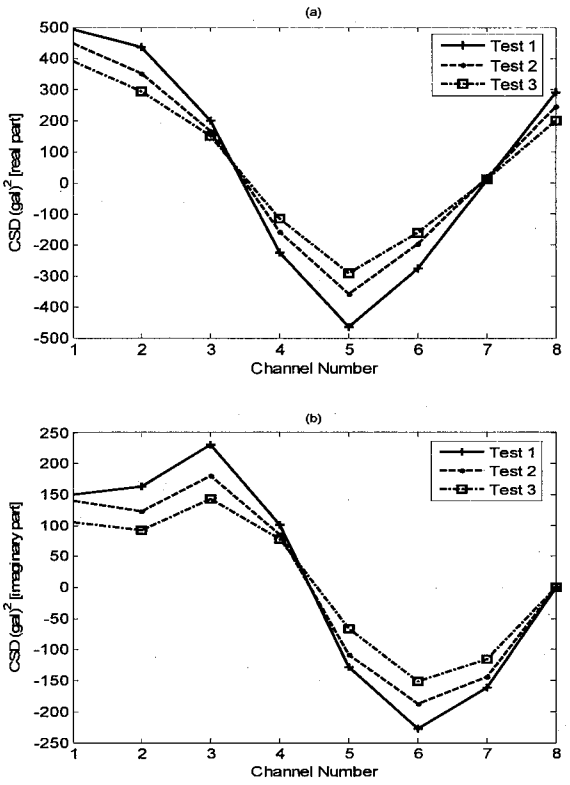

Fig. 9 CSD data at various channels estimated at frequency 530 Hz for damage case 1 using excitation frequency range of 500-600 Hz

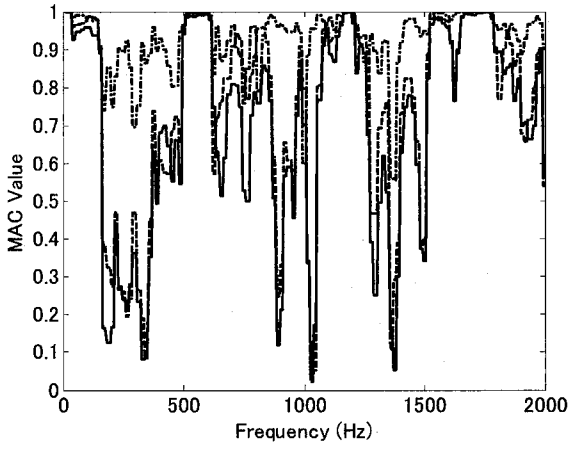

Fig. 10 MAC values for three combinations of CSD data obtained from damage case 1 using excitation frequency range of 500-600 Hz

It can also be noted that, MAC values are also close to unity in some frequency ranges other than the excitation frequency range (for example in the frequency range of about 1500 to 1750 Hz). When Figs. 10 and 11 are compared, it is clearly shown that MAC values are always close to unity within the excitation range and MAC values in the frequency of 1500-1750 Hz are not close to unity in case of using the excitation range of 600-700 Hz. It was also found that stable frequency ranges other than the excitation frequency range do not always exist in different circumstances such as changing damage location or structure type. Similar observations were noticed for the other excitation frequency ranges. From the previous observations it can be seen how the tunable piezoelectric actuator enriched the modal

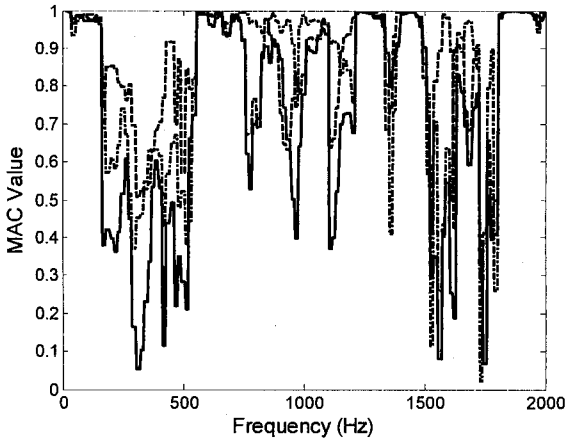

Fig. 11 MAC values for three combinations of CSD data obtained from damage case 1 using excitation frequency range of 600-700 Hz

data by introducing additional modal peaks to the response. Moreover, the influence of noise or measurement errors is minimized significantly within these additional peaks. Therefore, it was decided to use CSD data measured within the excitation frequency range and discarding other frequency ranges.

Figs. 12 through 16 show MAC values for the different excitation frequency ranges. In each figure MAC is used to compare CSD data for the following cases:

(I) Three different tests carried out on the RC column in damage case 1; {test 1 [D1] – test 2 [D1]} & {test 1 [D1] – test 3 [D1]} & {test 2 [D1] – test 3 [D1]}, indicated by thick solid lines.

(II) Three different tests carried out on the RC column in damage case 2; {test 1 [D2] – test 2 [D2]} & {test 1 [D2] – test 3 [D2]} & {test 2 [D2] – test 3 [D2]}, indicated by thin solid lines.

(III) Three different tests carried out on RC column in damage case 1 and three different tests carried out on RC column in damage case 2; {test 1 [D1] – test 1 [D2]} & {test 2 [D1] – test 2 [D2]} & {test 3 [D1] – test 3 [D2]}, indicated by dotted lines.

In Figs. 12 through 16, the thick solid lines are used to evaluate the repeatability of the experiment and the influence of noise and measurement errors for damage case 1, the thin solid lines are used to evaluate the repeatability of the experiment and the influence of noise and measurement errors for damage case 2, and the dotted lines are used to detect the occurrence of damage (due to cutting the steel bars in damage case 2). In other words, solid lines (either thick or thin lines) are used to examine the influence of noise and repeatability of the experiment while the dotted lines are used to detect the occurrence of damage. In a similar manner, MAC values that results from environmental changes or operational loads can be estimated for the intact structure. Thus, a threshold of the MAC values that results from noise, measurement errors, environmental changes or operational loads can be estimated. Then, MAC values smaller than the threshold can indicate the occurrence of damage. In Fig. 12, MAC values denoted by the solid lines are measured between about 0.9 and 1.0 in the frequency ranges of 305-330 Hz and 350-400 Hz which indicates very small influence of noise in these frequency ranges. On the other hand, MAC values denoted by the solid lines decreased to about 0.7

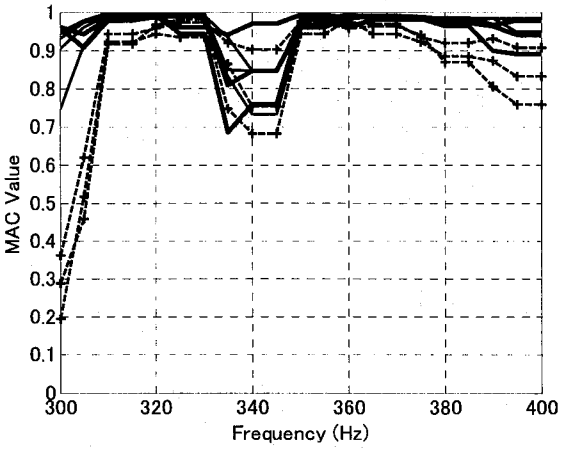

Fig. 12 MAC values for the RC column using excitation frequency range of 300-400 Hz

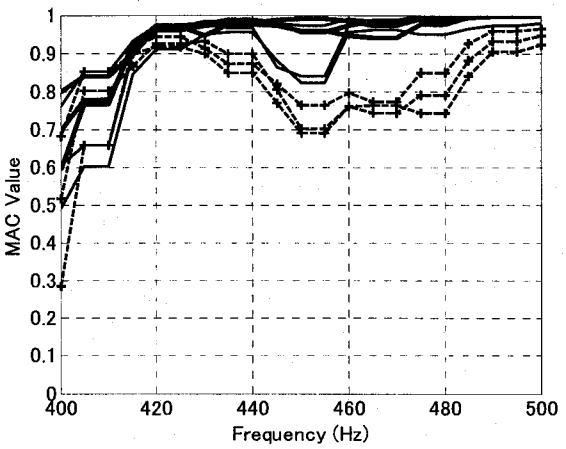

Fig. 13 MAC values for the RC column using excitation frequency range of 400-500 Hz

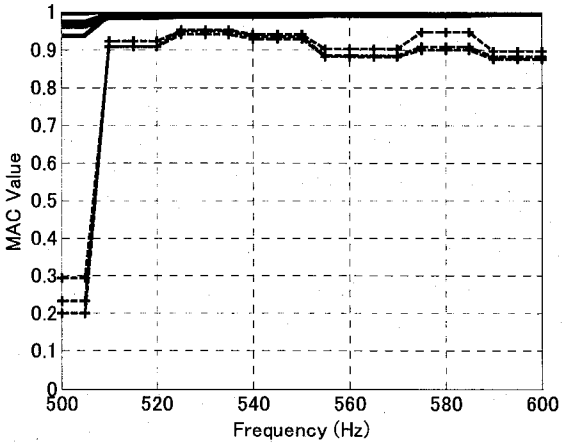

Fig. 14 MAC values for the RC column using excitation frequency range of 500-600 Hz

in the frequency ranges of 300-305 Hz and 330-350 Hz which indicates high influence of noise in these ranges. MAC values denoted by the dotted lines decreased below 0.7 in the frequency range of 300-305 Hz which indicates the occurrence of damage. The indication of damage could be observed only in the frequency range of 300-305 Hz which is relatively a small range compared to the total

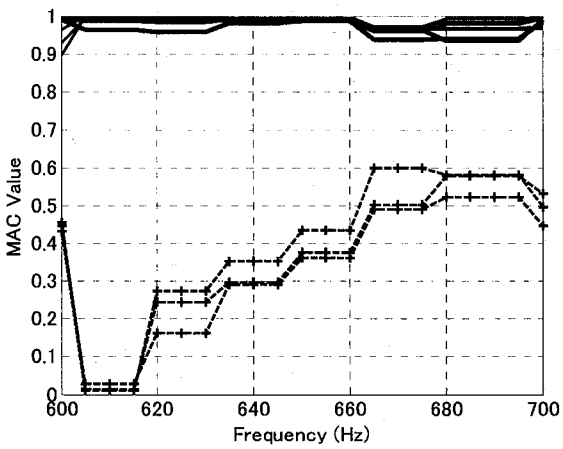

Fig. 15 MAC values for the RC column using excitation frequency range of 600-700 Hz

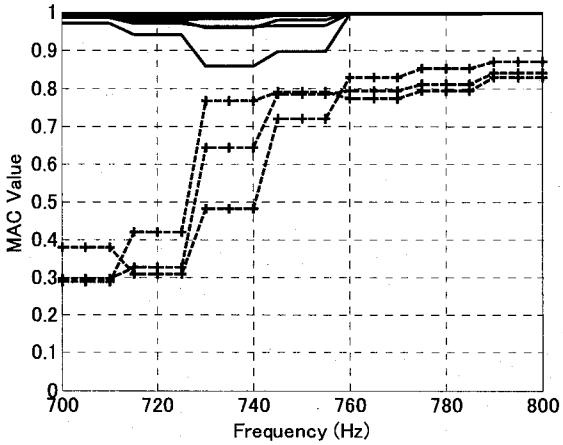

Fig. 16 MAC values for the RC column using excitation frequency range of 700-800 Hz

excitation range of 300-400 Hz. Moreover, the influence of noise in this range is high. Therefore, damage could not be detected with high confidence when the structure is excited in the frequency range of 300-400 Hz. Similar observations are noticed in Figs. 13 and 14. It should be noted that the results of Figs. 12, 13, and 14 are estimated using different excitation ranges and the experiment is carried out three times for each excitation range. Hence, MAC values at the end of Fig. 12 are different from those obtained at the beginning of Fig. 13 and so on. In Figs. 13 and 14, MAC values denoted by the dotted lines decrease below 0.7 in small frequency ranges at the beginning of the excitation frequency. In Fig. 15, the influence of noise is very small as the MAC values denoted by the solid lines are measured between 0.9 and 1.0 in the total excitation range from 600 to 700 Hz. Damage could be indicated very clearly in this figure as the MAC values decreased significantly below 0.6 in the total excitation range from 600 to 700 Hz. Another clear indication of damage is observed in the frequency range of 700-725 Hz, as shown in Fig. 16. In almost all figures, MAC values denoted by the solid lines are very close to 1, which indicates very small influence of noise and measurement errors in both damage cases. To conclude, in Figs. 12 through 14, although MAC values denoted by the dotted lines decreased slightly which

indicates to some extent the occurrence of damage, the indication of damage is not very clear and cannot be confirmed. On the other hand, in Figs. 15 and 16, MAC values, denoted by the dotted lines, decreased significantly which indicates very clearly the occurrence of damage. Fig. 15 showed the clearest indication of damage. Thus, it can be concluded that the excitation frequency range from 600 to 700 Hz was the most effective range in detecting the introduced damage.

5.2 Wall center

All procedures performed for the wall center are the same as those for the RC column. Figs. 17 through 21 show MAC values for the different excitation frequency ranges. In each figure MAC is used to compare CSD data for the following cases:

(I) Three different tests carried out on the wall center in damage case 1 ; {test 1 [D1] – test 2 [D1]} & {test 1 [D1] – test 3 [D1] } & {test 2 [D1] – test 3 [D1]}, indicated by thick solid lines.

(II) Three different tests carried out on the wall center in damage case 2; {test 1 [D2] – test 2 [D2]} & {test 1 [D2] – test 3 [D2]} & {test 2 [D2] – test 3 [D2]}, indicated by thin solid lines.

(III) Three different tests carried out on wall center in damage case 1 and three different tests carried out on wall center in damage case 2; {test 1 [D1] – test 1 [D2]} & {test 2 [D1] – test 2 [D2]} & {test 3 [D1] – test 3 [D2]}, indicated by dotted lines.

Figs. 17 and 18 show the clearest indication of damage for the wall center. As indicated in Fig. 17, the influence of noise is very small in the frequency range of 310-400 Hz as the MAC values denoted by the solid lines are measured above 0.9. MAC values denoted by the dotted lines decreased significantly below 0.7 in the frequency range of 300-330 Hz which shows clear indication of damage. Although, MAC values of the dotted lines are greater than 0.7 in the frequency range 330-400 Hz, the clear difference between the solid lines and dotted lines in this frequency range shows another indication of damage. In Fig. 18, MAC values denoted by the dotted lines decreased significantly below 0.4 in the frequency range of 430-500 Hz which shows very clear indication of damage. In Figs. 19, 20 and 21, although the influence of noise and measurement errors is high in several excitation frequency ranges, the influence of damage is more significant in these ranges as noted by the difference between the solid lines and dotted lines. Moreover, the very small values of the dotted lines observed in the frequency ranges of 500-550 Hz (Fig. 19), 645-700 Hz (Fig. 20), 700-730 Hz, and 750-785 Hz (Fig. 21) shows another indication of damage. Thus, it can be concluded that the excitation frequency ranges from 300 to 400 and from 400 to 500 Hz were the most effective ranges in detecting the introduced damage to the wall center.

5.3 Wall corner

Figs. 22 through 26 show MAC values for the wall corner using different excitation frequency ranges. In each figure MAC is used to compare CSD data for the following cases:

(I) Three different tests carried out on the wall corner in damage case 1 ; {test 1 [D1] – test 2 [D1]} & {test 1 [D1] – test 3 [D1] } & {test 2 [D1] – test 3 [D1]}, indicated by thick solid lines.

(II) Three different tests carried out on the wall corner in damage case 2; {test 1 [D2] – test 2 [D2]} & {test 1 [D2] – test 3 [D2]} & {test 2 [D2] – test 3 [D2]}, indicated by thin solid lines.

(III) Three different tests carried out on wall corner in damage case 1 and three different tests carried out on wall corner in damage case 2; {test 1 [D1] – test 1 [D2]} & {test 2 [D1] – test 2 [D2]} & {test 3

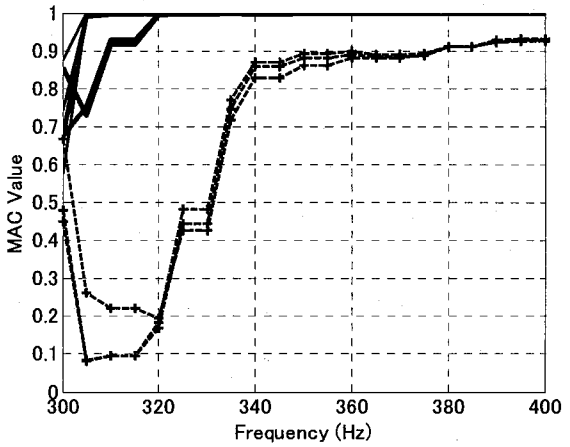

Fig. 17 MAC values for the wall center using excitation frequency range of 300-400 Hz

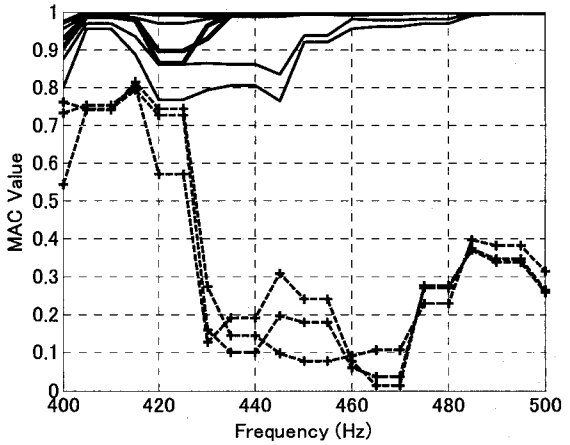

Fig. 18 MAC values for the wall center using excitation frequency range of 400-500 Hz

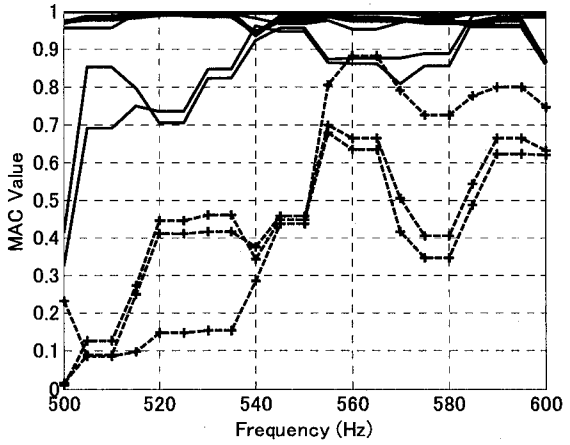

Fig. 19 MAC values for the wall center using excitation frequency range of 500-600 Hz

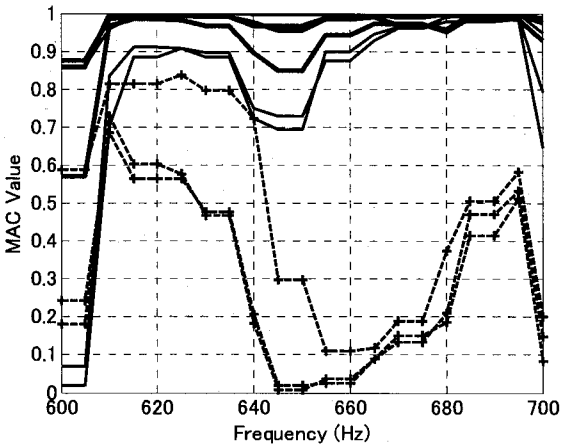

Fig. 20 MAC values for the wall center using excitation frequency range of 600-700 Hz

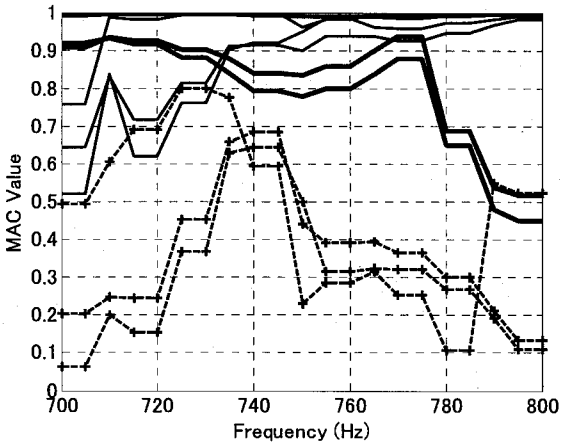

Fig. 21 MAC values for the wall center using excitation frequency range of 700-800 Hz

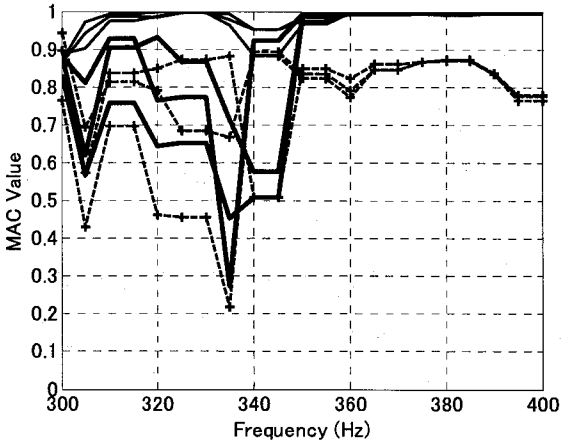

Fig. 22 MAC values for the wall corner using excitation frequency range of 300-400 Hz

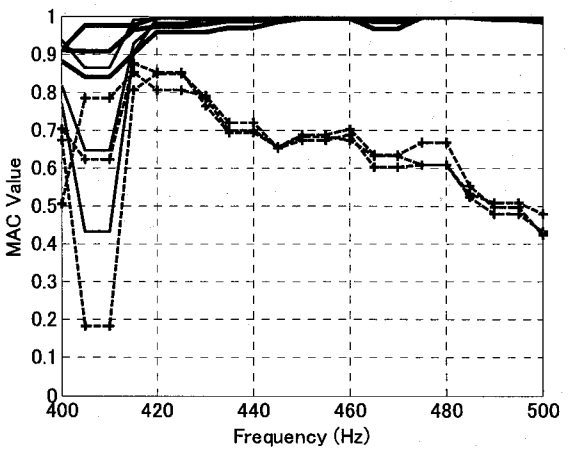

Fig. 23 MAC values for the wall corner using excitation frequency range of 400-500 Hz

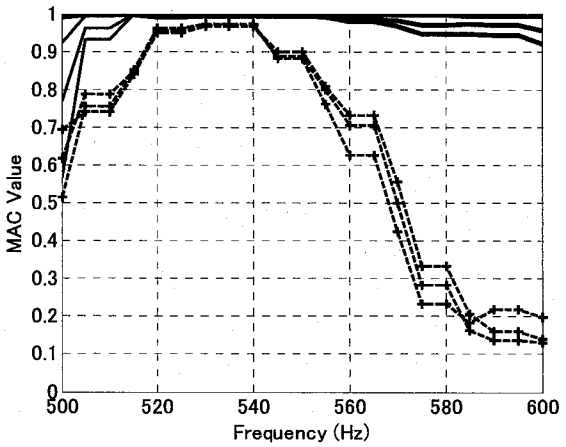

Fig. 24 MAC values for the wall corner using excitation frequency range of 500-600 Hz

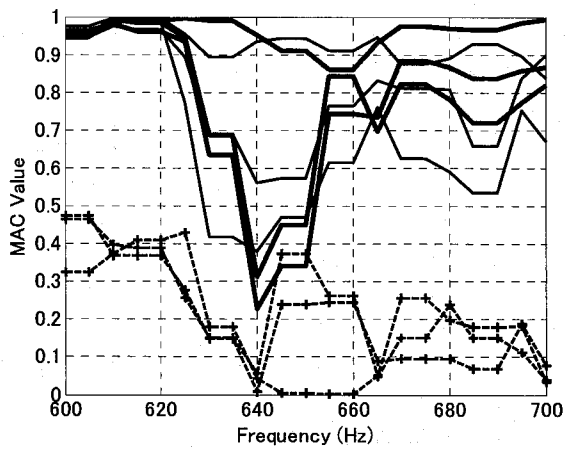

Fig. 25 MAC values for the wall corner using excitation frequency range of 600-700 Hz

[D1] – test 3 [D2]}, indicated by dotted lines.

As indicated in Fig. 22, the influence of noise is quite high and changes in MAC values that result from damage are very similar to those produced by noise. Hence, damage cannot be detected using the excitation range of 300-400 Hz. It should be noted that the same excitation frequency range of 300-400 Hz has shown very accurate results for the center location. Thus, it can be concluded that the effective excitation range in detecting the same damage type in the same structure may vary with changing damage location. Damage is best identified using the excitation frequency range of 400-500 Hz and 500-600 Hz, as shown in Figs. 23 and 24 respectively. In these figures, a clear difference between the solid lines and dotted lines can

be noticed in the frequency ranges of 425-500 Hz (Fig. 23) and 550-600 Hz (Fig. 24). Moreover, a significant decrease in MAC values of the dotted lines is also observed in the frequency range of 435-500 Hz (Fig. 23) and 565-600 Hz (Fig. 24). In Figs. 25 and 26, the influence of noise is high in some frequency ranges, but the changes in MAC values due to the occurrence of damage are usually higher as shown in the frequency ranges of 600-620 Hz, 655-700 (Fig. 25) and 700-705 Hz, 735-800 Hz (Fig. 26). It should be noted that the excitation range of 400-500 is effective in detecting damage for both damage location of the wall. By comparing the effective excitation frequency ranges for the column and the wall, it can be demonstrated that the effective frequency range is dependent on the structure type or geometry. Since it is very difficult to know in prior the most effective excitation frequency range for specific structure, it is recommended to excite the test structure with wide band of excitation frequencies.

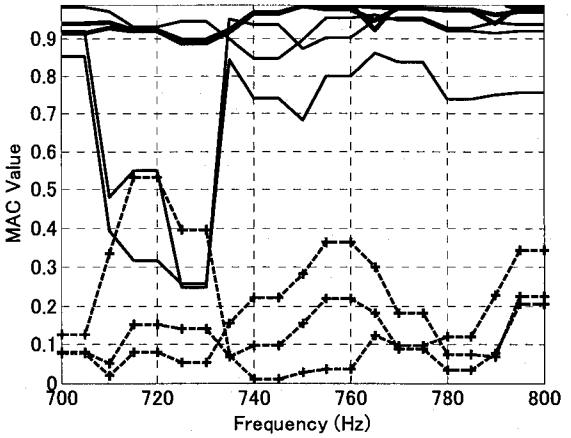

Fig. 26 MAC values for the wall corner using excitation frequency range of 700-800 Hz

6. Conclusions

In this research, a new methodology is developed to advance the state of the art of modal-based damage identification for structural health monitoring. The basic principle is to enrich the system modal measurements by integrating tunable piezoelectric actuator to the structure, and to sufficiently utilize the enriched information. With the integrated piezoelectric actuators, one can introduce additional resonant peaks into the system dynamic response in frequency domain and adjust them over the frequency band by tuning the wave generator. The proposed methodology is verified using the experimental data from concrete structures. Several observations and remarks can be concluded from the obtained results and are summarized as follows:

1. The influence of noise and measurement errors on the structure's dynamic response is minimized significantly within the excitation frequency range.
2. The changes in MAC values due to the presence of small damage are usually higher than the changes produced by the presence of noise and measurement errors.
3. The most effective excitation frequency range for detecting the damage is dependent on the structure type, structure geometry, damage type, and damage location. It is, therefore, necessary to excite the structure with wide band of excitation frequency since it is extremely difficult to know in prior the most effective excitation range for specific structure.
4. It is necessary to repeat the experiment several times to evaluate the changes in the dynamic response that result from repeatability of the experiment and presence of noise and measurement errors. In a similar manner, MAC values that results from environmental changes or operational loads can be estimated for the intact structure. Thus, a threshold of the MAC values that results from noise, measurement errors, environmental changes or operational loads can be estimated. Then, MAC values smaller than the threshold can indicate the occurrence of damage.

Acknowledgement

This research is supported by the Grant-in-Aids for Scientific Research, Ministry of Education. The authors wish to express their gratitude for this support. Special thanks are owed to Ms. Xinyu Li (Kitami Institute of Technology) for the preparation of the experimental setup.

References

1) Salawu O. S., Detection of structural damage through changes in frequency: a review, *Eng. Struct,* 19, pp. 718–723, 1997.
2) Stubbs N. and Osegueda R., Global non-destructive damage evaluation in solids, *Modal Anal.: Int. J. Analytical Exp. Modal Anal.* 5, pp. 67–79, 1990.
3) Stubbs N. and Osegueda R., Global damage detection in solids-experimental verification, *Modal Anal.: Int. J. Analytical Exp. Modal Anal.* 5, pp. 81–97, 1990.
4) Hearn G. and Testa R. B., Modal analysis for damage detection in structures, *J. Struct. Eng.* 117, pp. 3042–3063, 1991.
5) Salawu O. S. and Williams C., Structural damage detection using experimental modal analysis—a comparison of some methods, *Proc. 11th Int. Modal Anal. Conf. (Orlando, FL),* pp. 254–260, 1993.
6) Salawu O. S. and Williams C., Damage location using vibration mode shapes, *Proc. 12th Int. Modal Anal. Conf. (Honolulu, HI),* pp. 933–939, 1994.
7) Kam T. Y. and Lee T. Y., Detection of cracks in structures using modal test data *Eng. Fract. Mech.* 42, pp. 381–387, 1992.
8) Pandey A K, Biswas M. and Samman M. M., Damage detection from changes in curvature mode shapes, *J. Sound Vib.* 145, pp. 321–332, 1991.
9) Ho Y. K. and Ewins D. J., Numerical evaluation of the damage index, *Structural Health Monitoring 2000 (Palo Alto, CA),* pp. 995–1011, 1999.
10) Wang M. L., Xu F. L. and Lloyd G. M., Systematic numerical

analysis of the damage index method used for bridge diagnostics, *Proc. SPIE Symp. on Smart Structures and Materials: Smart Systems for Bridges, Structures, and Highways (Newport Beach, CA)* vol 3988 (Bellingham, WA: SPIE Optical Engineering Press), pp. 154–164, 2000.

11) Pandey A. K. and Biswas M., Damage detection in structures using changes in flexibility *J. Sound Vib.* 169, pp. 3–17, 1994.
12) Lin C. S., Unity check method for structural damage detection *J. Spacecr. Rockets* 35, pp. 577–579, 1998.
13) Reich G. W. and Park K. C., Experimental applications of a structural health monitoring methodology, *Proc. SPIE Symp. on Smart Structures and Materials: Smart Systems for Bridges, Structures, and Highways (Newport Beach, CA)* vol 3988 (Bellingham, WA: SPIE Optical Engineering Press), pp. 143–153, 2000.
14) Doebling S. W., Farrar C. R. and Prime M. B., Summary review of vibration-based damage identification methods, *Shock Vib. Digest* 30, pp. 91–105, 1998.
15) Doebling S. W., Farrar C. R., Prime M. B. and Shevitz D. W., Damage identification and health monitoring of structural and mechanical systems from changes in their vibration characteristics: a literature review, *Los Alamos National Laboratory Report* LA-13070-MS, Los Alamos, New Mexico, 1996.
16) Cornwell P., Kan M., Carlson B., Hoerst L. B., Doebling S. W. and Farrar C., Comparative study of vibration-based damage identification algorithms, *Proc.16th Int. Modal Anal. Conf. (Santa Barbara, CA)* pp 1710–6 (Part 2), 1998.
17) Dascotte E., Practical application of finite element tuning using experimental modal data, *Proc. 8th Int. Modal Anal. Conf. (Orlando, FL)*, pp. 1032–1037, 1990.
18) Friswell M. I. and Penny J. E. T., The practical limits of damage detection and location using vibration data, *Proc. 11th VPI&SU Symp. on Structural Dynamics and Control (Blacksburg, VA)*, pp. 31–40, 1997.
19) Cha P. D. and Gu W., Model updating using an incomplete set of experimental modes, *J. Sound Vib.* 233, pp. 587–600, 2000.
20) Nalitolela N. G., Penny J. E. T. and Friswell M. I., Mass or stiffness addition technique for structural parameter updating, *Modal Anal.: Int. J. Analytical Exp. Modal Anal.* 7, pp. 157–168, 1992.
21) Lew J-S and Juang J. N., Structural damage detection using virtual passive controllers, *J. Guid., Control, Dyn.* 25, pp. 419–424, 2002.
22) Hagood N. W. and von Flotow A., Damping of structural vibrations with piezoelectric materials and passive electrical networks, *J. Sound Vib.* 146, pp. 243–268, 1991.
23) Wu S., Piezoelectric shunts with a parallel R-L circuit for structural damping and vibration control, *Proc. SPIE Symp. on Smart Structures and Materials: Passive Damping and Isolation (San Diego, CA)* vol 2720 (Bellingham, WA: SPIE Optical Engineering Press), pp. 259–269, 1996.
24) Hollkamp J. J., Multimodal passive vibration suppression with piezoelectric materials and resonant shunts, *J. Intell. Mater. Syst. Struct.* 5, pp. 49–57, 1994.
25) Hagood N.W., ChungW. H. and von Flotow A., Modeling of piezoelectric actuator dynamics for active structural control, *Proc. 31st AIAA/ASME/ASCE/AHS/ASC Structures, Structural Dynamics and Materials Conf. (Long Beach, CA)*, pp. 2242–2256 (Part 4), 1990.
26) Agnes G. S., Development of a modal model for simultaneous active and passive piezoelectric vibration suppression, *J. Intell. Mater. Syst. Struct.* 6, pp. 482–487, 1995.
27) Tsai M. S. and Wang K. W., On the structural damping characteristics of active piezoelectric actuators with passive shunt, *J. Sound Vib.* 221, pp. 1–22, 1999.
28) Tang J., Liu Y. and Wang K. W., Semiactive and active–passive hybrid structural damping treatments via piezoelectric materials, *Shock Vib. Digest* 32, pp. 189–200, 2000.
29) Tang J. and Wang K. W., Vibration confinement via optimal eigenvector assignment and piezoelectric network, *J. Vib. Acoust., Trans. ASME* 126, pp. 27–36, 2004.
30) Beskhyroun S., Oshima T., Mikami S., and Tsubota Y., Structural Damage Identification Algorithm Based on Changes in Power Spectral Density, *Journal of Applied Mechanics, Japan Society of Civil Engineers (JSCE)*, Vol.8, pp. 73-84, 2005.
31) Farrar C. R. et al., Dynamic Characterization and Damage Detection in the I-40 Bridge Over the Rio Grande, *A Literature Review, Los Alamos National Laboratory Report, LA-12767- MS*, 1994.
32) Hayes M., *Statistical Digital Signal Processing and Modeling*, John Wiley & Sons, 1996.
33) Stoica P., and R.L. Moses, *Introduction to Spectral Analysis*, Prentice-Hall, Englewood Cliffs, NJ, pp. 52-54, 1997.
34) Welch P. D., The Use of Fast Fourier Transform for the Estimation of Power Spectra: A Method Based on Time Averaging Over Short, Modified Periodograms, *IEEE Trans. Audio Electro Acoustics*, Vol. AU-15, pp. 70-73, 1967.
35) Ewins D. J., *Modal Testing: Theory and Practice*, John Wiley, New York, 1985.

(Received: April 12, 2007)